Role of the Hyal−Cu (II) Complex on Bovine Aortic and Lymphatic Endothelial Cells Behavior on Microstructured Surfaces

ARTICLE *in* BIOMACROMOLECULES · JANUARY 2005

Impact Factor: 5.75 · DOI: 10.1021/bm049568g · Source: PubMed

6 AUTHORS, INCLUDING:

Rolando Barbucci
Università degli Studi di Siena
241 PUBLICATIONS **4,034** CITATIONS
SEE PROFILE

Stefania Lamponi
Università degli Studi di Siena
75 PUBLICATIONS **1,193** CITATIONS
SEE PROFILE

Agnese Magnani
Università degli Studi di Siena
104 PUBLICATIONS **1,712** CITATIONS
SEE PROFILE

Antonella Rossi
Università degli Studi di Siena
15 PUBLICATIONS **175** CITATIONS
SEE PROFILE

Role of the Hyal−Cu (II) Complex on Bovine Aortic and Lymphatic Endothelial Cells Behavior on Microstructured Surfaces

Rolando Barbucci,*,† Stefania Lamponi,† Agnese Magnani,† Federica M. Piras,† Antonella Rossi,‡ and Elisabetta Weber‡

C.R.I.S.M.A., Department of Chemical and Biosystems Sciences and Technologies and University Centre of Colle di Val d'Elsa, University of Siena 53 100 Siena, Italy, and Department of Neuroscience, Molecular Medicine Section, University of Siena, Via Aldo Moro 2, 53100 Siena, Italy

Received July 28, 2004; Revised Manuscript Received October 14, 2004

The ability of micropatterned surfaces to modulate cell behavior is combined with the well-known angiogenic property of the hyaluronan−Cu (II) complex. Hyaluronan−Cu (II) microstripes 100 and 25 μm wide on aminosilanised glass substrates were fabricated by photoimmobilization following two different methods: i.e., method I consisting in the photoimmobilization of the Hyal−Cu (II) complex; and method II based on the photoimmobilization of Hyal followed by the coordination with Cu (II). The chemistry and topography of the fabricated micropatterned samples were investigated by ATR FT-IR, atomic absorption, AFM, SEM, and ToF-SIMS. ATR FT-IR analysis demonstrated that hyaluronan conjugated with a photoreactive moiety was able to coordinate Cu (II) ions and that the photoimmobilization process was successful, as indicated by the intensity decrease of the IR band of the azidic group after the photoreaction. AFM and SEM images showed that reproducible Hyal−Cu (II) microstructures with both chemical and topographical heterogeneities have been obtained by the two preparation methods. The distribution of copper on the fabricated Hyal−Cu (II) microstructures has been investigated by ToF-SIMS. In both ToF-SIMS images and spectra, on Hyal−Cu (II) microstructures prepared by method I, the Cu peak (63 *m*/*z*) was detected only on the Hyal−Cu (II) microstripes, while on Hyal−Cu (II) microstructures prepared by method II, the Cu peak showed the same intensity both on the Hyal−Cu (II) microstripes and on the aminosilanised glass substrate, in agreement with the higher amount of Cu revealed by atomic absorption. The influence of Hyal−Cu (II) micropatterned surfaces on BAEC and LEC, in terms of migration and adhesion, has been analyzed. The results obtained indicate that Hyal−Cu (II) influences BAEC behavior inducing cell migration, while it is devoid of any effect on LEC.

Introduction

Angiogenesis is the growth of new blood vessels from preexisting ones. This process depends on many biomolecules such as growth factors and cytokines, able to stimulate endothelial cells adhesion, movement, and proliferation. Many of the vascular growth factors are polypeptides (e.g., vascular endothelial growth factor and transforming growth factor) and lipid molecules (e.g., prostaglandin E1).[1,2] In angiogenesis, a central role is played also by the extracellular matrix components (e.g., collagen and fibronectin), oligoelements and metals such as Cu (II),[3] a fundamental constituent of enzymes and proteins. It is well-known that Cu (II) is coordinated by many biological molecules, such as heparin or ceruloplasmin,[4] which is an angiogenic inducer in vivo, and that at micromolar concentration, it affects cell migration and proliferation.[5−7] The role of Cu (II) in stimulating angiogenesis is probably due to its effect to mediate the interaction between endothelial cells and an angiogenic factor: angiogenin.[8] This protein, binding specifically to the surface of endothelial cells,[9] can induce most of the events necessary for the formation of new blood vessels.

As previously reported,[10,11] hyaluronic acid (Hyal) is able to coordinate Cu (II) ions and the resulting complex favors cell migration in vitro. Moreover, in vivo tests demonstrated that the Hyal−Cu (II) hydrogel complex induces a remarkable neovascularisation.[10,11]

Micropatterned surfaces have shown to influence processes extremely important in tissue and organ formation, such as adhesion and migration of specific cells.[12−17] Previous studies demonstrated that hyaluronic acid photoimmobilized on aminosilanised glass does not provide an adhesive substrate for many cell types; the cells, in fact, adhered on aminosilanised glass microdomains.[13,14,17]

The aim of this study was to evaluate whether the presence of Cu (II) involved in the coordination with Hyal could improve the cell affinity for Hyal microstructures, favoring cell adhesion and migration. Two different cell lines were tested, namely, bovine aortic endothelial cells (BAEC) and lymphatic endothelial cells (LEC).

* To whom correspondence should be addressed. Phone: +39-0577-234382. Fax: +39-0577-234383. E-mail: barbucci@unisi.it.

† C.R.I.S.M.A., Department of Chemical and Biosystems Sciences and Technologies, and University Centre of Colle di Val D'Elsa.

‡ Department of Neuroscience, Molecular Medicine Section.

10.1021/bm049568g CCC: $30.25
Published on Web 12/08/2004

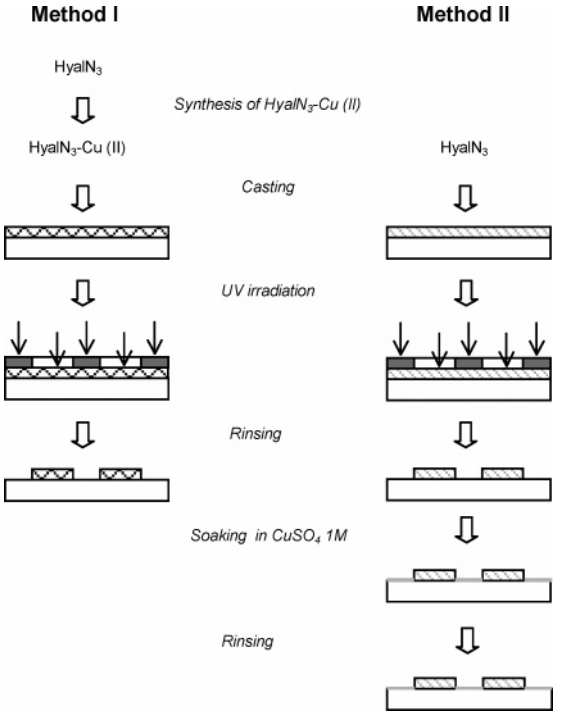

Figure 1. Scheme of the two photoimmobilization methods used to fabricate Hyal−Cu (II) microstructures on aminosilanised glass substrates.

Experimental

Materials. Sodium salt of hyaluronic acid (MW ≅ 150−200 kDa) was supplied by Biophil Italia S.p.A. (Milano, Italy). 4-Azidoaniline hydrochloride, 1-ethyl-3-[3-(dimethylamino)propyl] carbodiimide hydrochloride (EDC), 3-aminopropyl-3aminoethyl-trimethoxysilane, cupric sulfate pentahydrate, and all the solvents used were purchased from Fluka Chemie AG (Switzerland). Cell culture reagents were purchased from Sigma-Aldrich (Milano, Italy).

Fabrication of Hyal−Cu (II) Micropatterned Surfaces. The photoimmobilization method used in this study has been previously described in details.[14] The macromolecule to be photoimmobilized needs to be conjugated with a photoreactive moiety; therefore, hyaluronan has been conjugated with azidoaniline, chosen as photoreactive unit. The photoreactive macromolecule is from now on indicated as $X-N_3$, i.e., Hyal-N_3, HyalN_3−Cu (II). To improve their hydrophilic properties the glass substrates were aminosilanised.[13,14]

The Hyal−Cu (II) microstructures analyzed in this work have been fabricated by following two preparation methods (Figure 1):

Method I. The HyalN_3−Cu (II) complex has been synthesized in solution by mixing a HyalN_3 aqueous solution (1 mg/mL) with a 1M $CuSO_4$ solution for 24 h in a molar ratio of 1:1. The final solution was then dialyzed using a dialysis tube with a 12000 MW cutoff and then lyophilized. A thin film of HyalN_3−Cu (II) was cast on the aminosilanised glass substrates. After drying at room temperature in the dark, Hyal−Cu (II) microstripes were prepared by irradiating the samples for 30 s with an UV source (Helios Italquarz GRE 400W) at a distance of 40 cm, using a chromium-quartz photomask with a pattern of 10, 25, 50, and 100 μm stripes. After removing the photomask, the samples were rinsed with distilled water.

Method II. HyalN_3 microstripes on aminosilanised glass substrates were fabricated following the procedure reported for method I. The fabricated HyalN_3 microstructures were then soaked for 24 h in a 1M $CuSO_4$ aqueous solution to allow the Hyal−Cu (II) complex formation. The Hyal−Cu (II) micropatterned samples obtained were then soaked in distilled water for 48 h to remove the unbound copper ions.

Attenuated Total Reflection Infrared Spectroscopy (ATR FT-IR). Infrared spectra were collected using an FT-IR spectrometer (FTS 6000 Biorad, Bio-Rad Hercules, CA) equipped with the apparatus for ATR experiments and a light microscope (UMA 500 Biorad). The internal reflection element used was a germanium single reflection crystal with a 45° incidence angle. ATR FT-IR spectra have been collected on powdered samples and on thin films cast from aqueous solutions on glass by acquiring 64 scans from 4000 to 800 cm^{-1}, with 2 cm^{-1} resolution. A mercury cadmium telluride (MCT) detector was used. The ATR FT-IR spectra are reported as acquired.

Atomic Absorption. The quantitative analysis of Cu on the fabricated Hyal−Cu (II) microstructures was performed using an Analist 100 HGA-800 (Perkin-Elmer, Wellesley, MA) atomic absorption spectrometer equipped with an automated sampling system (Autosampler AS-72). The absorbance measurements were carried out on diluted solutions obtained by dissolving the Hyal−Cu (II) microstructures using an HNO_3/H_2O_2 (30%) mixture (1:1 v/v). The absorbance versus concentration (μg/L) calibration curve was determined by following a standard procedure.[18]

Time-of-Flight Secondary Ion Mass Spectrometry (ToF-SIMS). ToF-SIMS analysis of the Hyal−Cu microstructures was carried out with a TRIFT III time-of-flight secondary ion mass spectrometer (Physical Electronics, Chanhassen, MN) equipped with a $^{69}Ga^+$ liquid-metal primary ion source. Positive and negative ion images were acquired with a pulsed, unbunched 25 keV primary ion beam at 600 pA by rastering the ion beam over a 300 μm × 300 μm sample area. The primary ion dose was kept below 10^{13} ions/cm^2 to maintain static SIMS conditions. Charge compensation was achieved by using a pulsed, low-energy electron flood gun. The data were acquired in raw data stream mode. Positive data were calibrated to CH_3^+ (15.023 *m*/*z*), $C_2H_3^+$ (27.023 *m*/*z*), and $C_3H_5^+$ (41.039 *m*/*z*); negative data were calibrated to CH^- (13.008 *m*/*z*), OH^- (17.003 *m*/*z*), and C_2H^- (25.008 *m*/*z*). Region-of-interest (ROI) analysis was performed by extracting spectra from defined areas of interest in the ToF-SIMS images. ToF-SIMS images are reported as acquired.

Atomic Force Microscopy (AFM). The microstructures morphology was analyzed with an Explorer atomic force microscope (ThermoMicroscope, Veeco Instruments, NY). Before AFM analysis, the microstructured samples were cleaned under a nitrogen flow. AFM images were acquired on different areas of the samples by operating in contact mode, using an etched Si_3N_4 probe with a constant force of 0.032 N/m, in air.

Scanning Electron Microscopy (SEM). For SEM analysis, the microstructured samples were mounted on alumina stubs and sputter-coated with gold using an automatic sputter

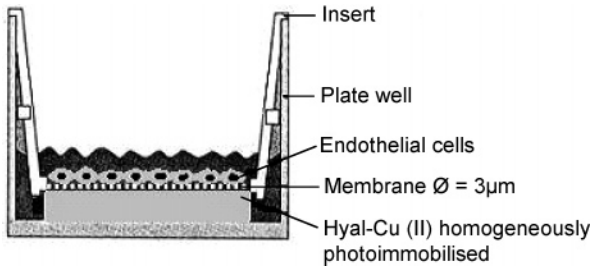

Figure 2. Scheme of the well plate used for chemotaxis experiments.

coater (BAL-TEC SCD 050, Balzer, Germany). An XL 20 scanning electron microscope (Philips, The Netherlands) operating at 15 kV accelerating voltage was used to analyze the Hyal−Cu (II) 100 μm wide microstripes on glass and all the Hyal−Cu (II) microstructures used for the cell culture experiments.

Cell Cultures. Bovine aortic endothelial cells (BAEC) and lymphatic endothelial cells (LEC) were obtained from bovine thoracic aorta and bovine thoracic duct, respectively, by enzymatic digestion with 0.05% collagenase (type 2; 239 U/mg; Worthington, Lakewood, NJ) and cultured in 25 cm^2 Falcon flasks in Dulbecco's modified eagle medium (DMEM Sigma, St. Louis, MO) supplemented with 20% FCS (GIBCO, Life Technologies Ltd, Paisley, Scotland, U.K.), 100 μg/mL endothelial cell growth supplement (ECGS, Sigma), and 2 mM glutamine (Sigma).[19] At confluence, cells were trypsinised and seeded on the Hyal−Cu (II) micropatterned surfaces.

Adhesion and Proliferation Assay. To evaluate the ability of the Hyal cupric complex to influence cell adhesion, endothelial cells were seeded on ethanol-sterilized and HEPES saline-treated microstructured aminosilanised glass at a density of 7×10^3 cells/200 μL. Hyal−Cu (II) 100 and 25 μm micropatterned samples were incubated at 37 °C. Fresh medium was added when the cells had adhered to the microstructures and thereafter replaced every other day.[14] Cell behavior on the micropatterned surfaces was monitored using a phase contrast microscope (Olympus IX71) equipped with a digital camera. Cell monitoring and counting were performed after 24 and 48 h, using 10X and 40X magnification. Cell morphology was evaluated by SEM following the procedure reported by Greco et al.[20] Area and perimeter of the adhered cells were determined by SEM to evaluate cell's affinity for the substrate. Fifty cells were analyzed for each microdomain using the NHI Image software (available online at http://rsb.info.nih.gov/nhi.image/), and the obtained data were elaborated using the Origin Pro 7.0 software (Origin Lab Corporation).

Chemotaxis Assay. Chemotaxis experiments were performed using 24-well plates and cell culture inserts (3.0 μm pore size PET track-etched membrane, Corning, USA), as reported in Figure 2.

Three different samples were analyzed, i.e., Hyal, Hyal−Cu (II) prepared according to method I and Hyal−Cu (II) prepared following method II; all of them were homogeneously photoimmobilized. First the samples were placed on the bottom of the well; then 1×10^5 cells, suspended in 1 mL of DMEM containing 2% FCS, were placed on the PET membrane of the insert. DMEM containing 2% FCS was used as a negative control and complete M199 containing 10% FCS as a positive control. After 6 h of incubation at 37 °C, the upper surface of the filter was scratched in order to remove the nonmigrated cells as previously described.[1] The cells migrated across the PET membrane pores were counted using a light microscope on 5 randomly selected areas on each sample.

Results and Discussion

Hyal−Cu (II) microstructures on aminosilanised glass substrates able to modulate cell behavior were fabricated by photoimmobilization following two preparation methods. The realized Hyal−Cu (II) microstructures showed both the ability of Hyal microstripes on aminosilanised glass to modulate cell behavior, favoring cell adhesion and migration[13,14,17] and the angiogenic properties of the Hyal−Cu (II) complex.[7]

Characterization of HyalN_3−Cu (II) by ATR FT-IR. ATR FT-IR spectroscopy was used to examine the structure of the synthesized HyalN_3−Cu (II) complex. In Figure 3a, the ATR FT-IR spectrum of the HyalN_3−Cu (II) complex is compared to that of HyalN_3. The HyalN_3−Cu(II) ATR FT-IR spectrum shows all the characteristic IR peaks expected for the HyalN_3 compound, except for the maximum of the broad band due to the overlapping of the COO^- and amide C═O stretching peaks,[13] which is shifted to higher wavenumbers (from 1609 to 1630 cm^{-1}) in the HyalN_3−Cu (II) spectrum. This shift might be due to an interaction between the C═O amidic group and the cupric ion, indicating that Cu (II) is bound to the amidic C═O groups of the HyalN_3 polymer. A bond between the Cu (II) ion and the COO^- group is not excluded.

In a previous work,[21] for the Hyal−Cu (II) complex not photoreactive (i.e., unbound to azido-aniline) in aqueous solution, a 4+2 structure was hypothesised, in which both the amidic C═O and the carboxyl group are involved in the coordination site. The azido-aniline, used to synthesize the photoreactive polymer, binds to the Hyal carboxyl groups, so that in HyalN_3 the number of free carboxyl groups (which can interact with Cu(II)) is drastically decreased with respect to the native Hyal. The structural configuration of HyalN_3−Cu (II), thus, may be no longer that required for the 4+2 coordination, where an amidic C═O, a COO^- group, and two water molecules are bound to the cupric ion. From the HyalN_3−Cu (II) ATR FT-IR spectrum it can be assumed that Cu (II) is bound to the amidic C═O groups of the HyalN_3 polymer.

The Hyal−Cu (II) complex ATR FT-IR spectrum acquired after photoimmobilization does not show any difference compared to that collected before UV irradiation (Figure 3b), indicating that no structural changes occur during the photoimmobilization process. The same structure is suggested for the Hyal−Cu (II) complex before and after the photoimmobilization on glass substrates.

In the Hyal−Cu (II) ATR FT-IR spectrum (Figure 3b), the intensity decrease of the band at 2130 cm^{-1}, assigned to the azidic group, indicates that the photoimmobilization process was successful.

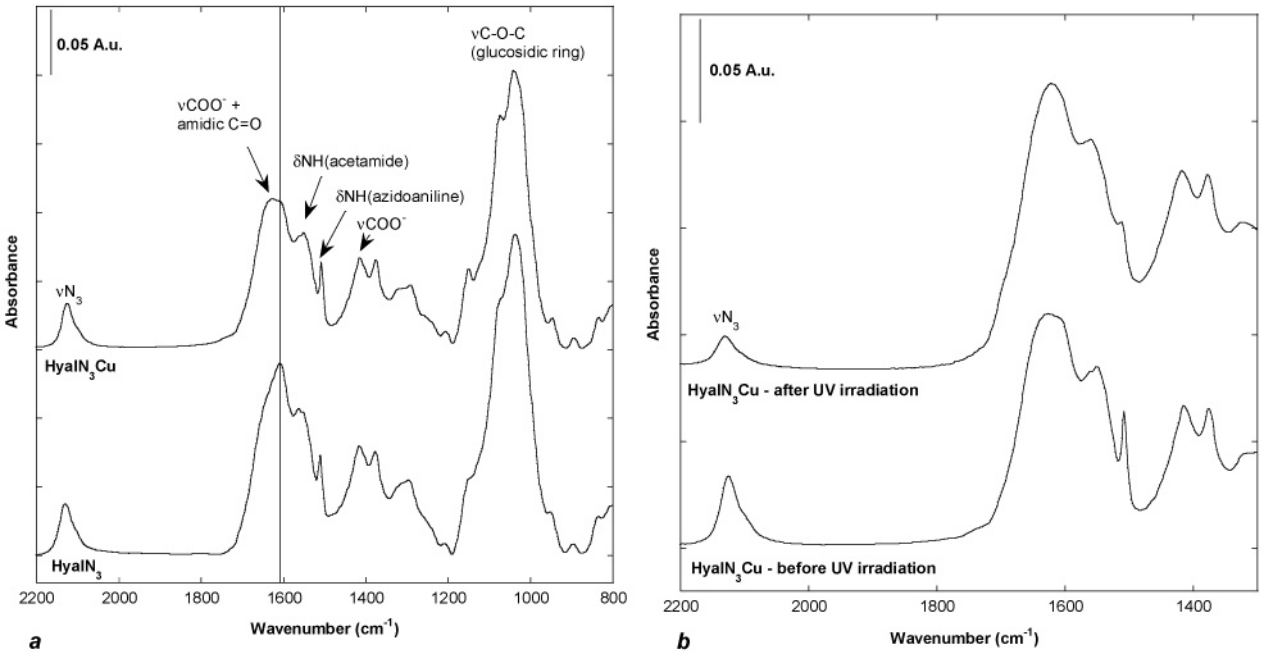

Figure 3. ATR FT-IR spectra of $HyalN_3$ and $HyalN_3$−Cu (a). Spectra acquired on powdered samples after lyophilization. ATR FT-IR spectra of $HyalN_3$−Cu before and after photoimmobilization on glass substrates (b). Spectra acquired on thin films cast on aminosilanised glass.

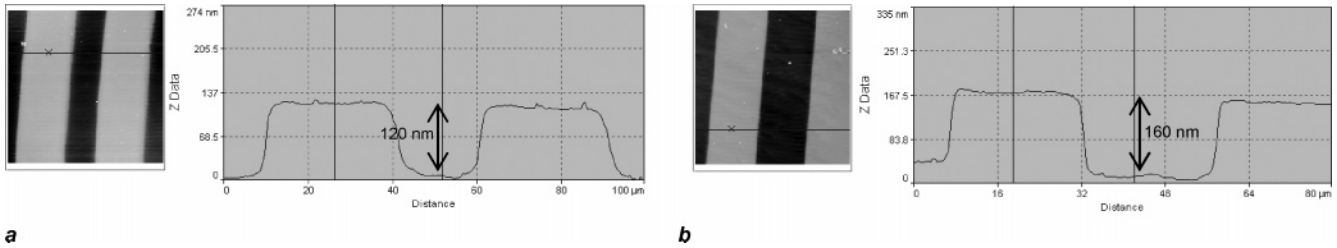

Figure 4. AFM images of $HyalN_3$−Cu (II) microstripes 25 μm wide on aminosilanised glass substrates. In panels a and b are shown the AFM image of the microstructures fabricated following method (I) and method (II), respectively. Images are 100 μm × 100μm (a) and 80 μm × 80 μm (b).

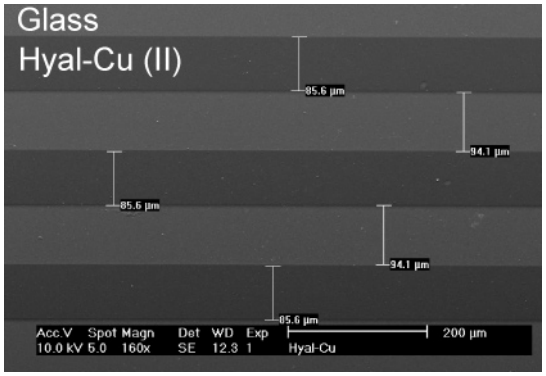

Figure 5. SEM image of Hyal−Cu (II) microstripes 100 μm wide on aminosilanised glass.

Topographical Characterization of Hyal−Cu (II) Microstructures by AFM and SEM. Hyal−Cu (II) microstripes on glass were realized following two fabrication methods consisting in the Hyal−Cu (II) complex formation before (method I) and after (method II) the photoimobilization step (Figure 1). Microstructured surfaces consisting of Hyal−Cu (II) microstripes 100 and 25 μm wide on glass substrates have been fabricated. The topography of the Hyal−Cu (II) microstructures was analyzed by AFM and SEM. As shown in Figures 4 and 5, the morphology of the Hyal−Cu (II) microstripes is regular in space and the domain areas are quite sharp. Hyal−Cu (II) microstructures fabricated following method I are 120 nm thick (Figure 4a); those obtained by method II are 160 nm thick (Figure 4b). The step edge of the stripes is gently sloped from the top to the bottom of the grooves, determining a difference of about 5 μm between the top and the bottom widths. In Figure 5, the SEM micrograph of Hyal−Cu (II) microstripes 100 μm wide is reported. Topographical analysis of microstripes 100 μm wide could not be done by AFM since the maximum scan area in the Explorer atomic force microscope is 100 μm.

Table 1. Quantitative Determination of Cu on Hyal−Cu (II) Microstructures by Atomic Absorption[a]

	Hyal−Cu (II) (method I)	Hyal−Cu (II) (method II)
Cu μg/50 μg of Hyal	2.1 ± 0.2 μg	2.7 ± 0.2 μg

[a] The Hyal−Cu (II) microstructures were prepared according to method I and method II as shown in Figure 1.

Quantitative Determination of Cu by Atomic Absorption. The amount of Cu (II) on the fabricated Hyal−Cu (II) microstructures was determined by atomic absorption. The quantity of Cu (II) analyzed corresponds to 4:1 molar ratio between the disaccharide unit and Cu (II). As reported in Table 1, the quantity of Cu (II) is slightly different for the two classes of samples. The slightly higher amount found

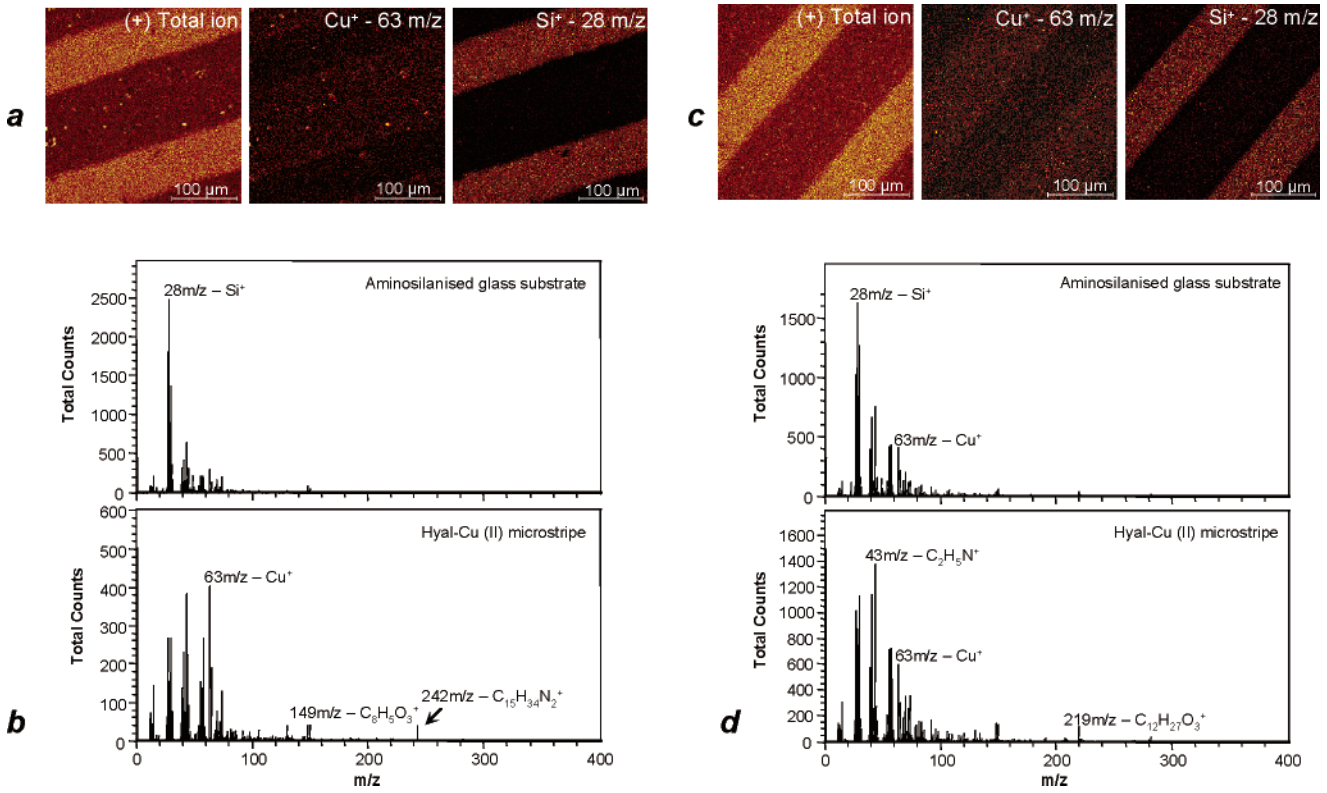

Figure 6. Positive ion ToF-SIMS images of Hyal−Cu (II) microstripes 100 μm wide on aminosilanised glass. Sample prepared according to method I (a) and method II (c). Images are 300 μm × 300 μm. Positive ion ToF-SIMS ROI spectra of Hyal−Cu (II) microstructures prepared following method I (b) and method II (d). The positive ion ToF-SIMS ROI spectra were extracted from the Hyal−Cu(II) microstripe (bottom) and from the aminosilanised glass substrate (up) in the total ion ToF-SIMS image.

on the samples prepared by method II may be due to Cu (II) bound to the terminal aminic groups present on the aminosilanised glass substrate, as confirmed by atomic absorption analysis of aminosilanised glass soaked, first, in a 1 M $CuSO_4$ solution for 24 h and then in water for 48 h. After rinsing with distilled water, the quantity of Cu (II) detected by atomic adsorption was 8,6 ng/mm^2. Cu (II) ions show a high affinity to the aminic groups on the aminosilanised glass surface.[13,14]

Surface Chemical Characterization of Hyal−Cu (II) Microstructures by ToF-SIMS. In Figure 6a, the ToF-SIMS images of total ion, Cu (63 *m/z*) and Si (28 *m/z*) acquired on Hyal−Cu (II) microstructures realized according to method I are presented. The distribution of Cu and Si (glass substrate) on the microstructures is shown. In ToF-SIMS images, brighter pixels correspond to a higher intensity of the element peak. It can be observed that the intensity of the Cu peak is higher on the Hyal−Cu stripes, whereas the intensity of the Si peak is higher on the substrate, i.e., between the stripes. The positive ion ToF-SIMS ROI spectra extracted from different regions in the total ion ToF-SIMS image are shown in Figure 6b. The positive ion ToF-SIMS ROI spectrum extracted from the Hyal−Cu stripe area shows the Cu and the Hyal characteristic peaks.[13] These peaks were not observed in the ROI spectrum extracted from the substrate area, which, instead, shows the Si peak and other peaks characteristic of the aminosilanised glass substrate. The ToF-SIMS images of the total ion, Cu and Si collected on Hyal−Cu (II) microstructures fabricated according to method II are reported in Figure 6c. The distribution of Cu and Si on the microstructures is shown. The intensity of the Cu peak is almost equal on the whole analyzed area; the intensity of the Si peak is higher on the substrate between the Hyal−Cu stripes. In Figure 6d, the positive ion ToF-SIMS ROI spectra extracted from different regions in the total ion ToF-SIMS image are presented. The Cu peak at 63 *m/z* was detected in both the positive ion ToF-SIMS ROI spectrum extracted from the Hyal−Cu stripe area and the ROI spectrum extracted from the substrate stripe area.

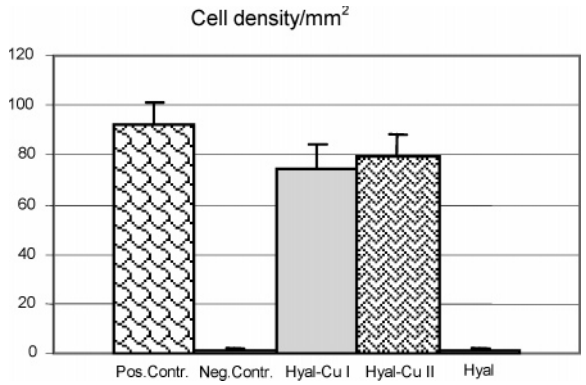

Figure 7. Chemotaxis of BAEC. Cell density/mm^2 on Hyaluronan (Hyal) and Hyal−Cu (II) prepared according to both method I and method II (Hyal−Cu I and Hyal−Cu II). The analyzed samples were thin films homogeneously photoimmobilized on aminosilanised glass substrates. DMEM containing 2% FCS and complete M199 containing 10% FCS were used as negative and positive control, respectively. The data were acquired 6 h after starting the experiment. The maximum semi-dispersion is adopted for the error bar.

Both ToF-SIMS images and ToF-SIMS ROI spectra indicate that on Hyal−Cu (II) microstructures prepared by

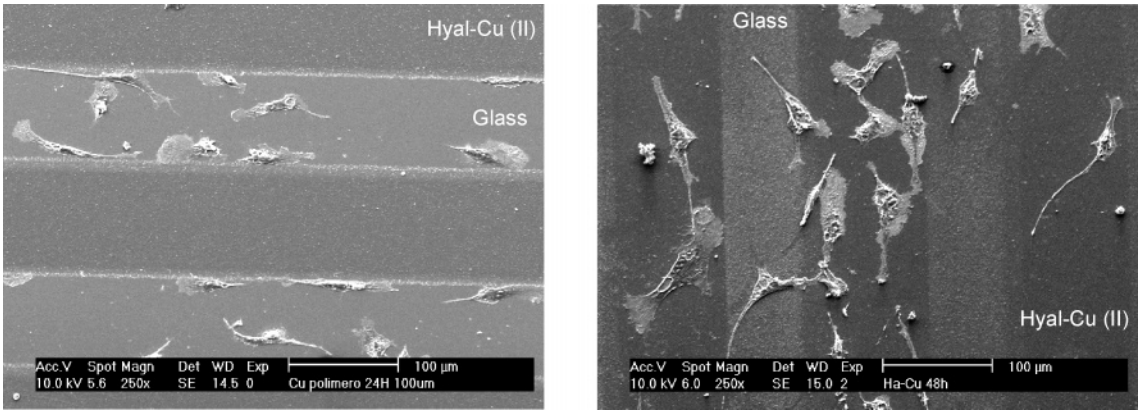

Figure 8. SEM micrographs of BAEC adhered to HyalN_3−Cu (II) microstripes on aminosilanised glass. After 24 h of culture (left), BAEC are aligned on the substrate adhering on the edge of the Hyal−Cu (II) microstripes. After 48 h of culture (right), the cells extended their pseudopodia on the Hyal−Cu (II) microstripes and adhered on them.

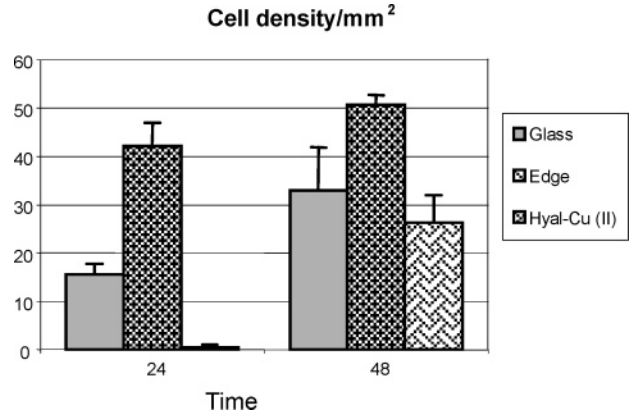

Figure 9. Cell density/mm^2 as a function of time for BAEC cultured on Hyal−Cu (II) 100 μm microstripes on aminosilanised glass. Left, aminosilanised glass substrate (Glass); middle, edge of the Hyal−Cu (II) microstripes (Edge); right, Hyal−Cu (II) microstripes (Hyal−Cu (II)). The maximum semidispersion is adopted for the error bar.

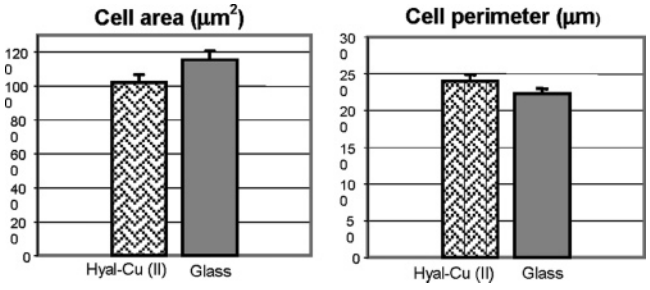

Figure 10. BAEC area (left) and perimeter (right) after 48 h of culture on Hyal−Cu (II) 100 μm microstripes (Hyal−Cu (II)) and on aminosilanised glass substrate (Glass). The maximum semi-dispersion is adopted for the error bar.

method I, Cu is detected only on the Hyal−Cu (II) microstripes. On Hyal−Cu (II) microstructures prepared by method II, the Cu peak showed the same intensity both on the Hyal−Cu (II) microstripes and on the aminosilanised glass substrate, in agreement with the atomic absorption results.

Chemotaxis Assay Using BAEC and LEC. Chemotaxis experiments were carried out on HyalN_3 and Hyal−Cu (II) samples prepared according to both method I and method II. The analyzed samples were thin films homogeneously photoimmobilized on aminosilanised glass substrates. As shown in Figure 7, the number of BAEC migrated through the pores of the filter is about the same for both Hyal−Cu (II) samples (i.e. Hyal−Cu (II) method I and Hyal−Cu (II) method II). The number of migrated cells on the positive control (i.e. complete M199 containing 10% FCS) is slightly higher than that on the Hyal−Cu (II) samples. No migrated cells were observed on Hyal. On the contrary, LEC were not influenced by the presence of Cu (II) coordinated to Hyal; in fact, chemotaxis assay demonstrated that there are no migrated cells for both samples obtained by the two preparation methods (data not shown).

Cell Behavior on Hyal−Cu (II) Microstripes 100 and 25 μm Wide. BAEC and LEC were used to test how the chemical and topographic features of Hyal−Cu (II) microstructures on aminosilanised glass influence cells behavior. On Hyal−Cu (II) microstripes 100 μm wide, after 24 h, BAEC adhered on the aminosilanised glass stripes, preferentially on the edge (Figure 8a). After 48 h, the cells extended their pseudopodia and moved along the Hyal−Cu (II) microstripes (Figure 8b). As shown in Figure 9, at 48 h an increment of cell density on the whole sample was observed. The maximal effect was achieved on the Hyal−Cu (II) microstripes, where an increase of about 25 units was detected. The smallest increment of cell number was found on the edge. Probably the cells, while moving from aminosilanised glass to Hyal−Cu (II), adhered first to the edge of the stripes and then moved to the polymer microstripes.

To evaluate the degree of affinity of the adhered cells for the substrate, cell perimeter and area were calculated. The results were compared to those obtained for the aminosilanised glass which is known to be a good substrate for cell adhesion. As shown in Figure 10, no significant differences in cell morphology were detected on aminosilanised glass substrates compared to Hyal−Cu (II) microstripes 100 μm wide. On the contrary, LEC kept adhering only on aminosilanised glass even after 48 h of culture, they never moved to Hyal−Cu (II) microstripes and did not significantly proliferate either on the samples prepared by method I or in those prepared by method II (Figure 11).

Chemotaxis experiments performed on homogeneous Hyal and Hyal−Cu (II) thin films indicate that Hyal−Cu (II), unlike Hyal, significantly increased cell chemotaxis, independently from the preparation method. The biological data indicate that hyaluronan coordinated to Cu(II) favors cell adhesion and migration of BAEC as shown by migration

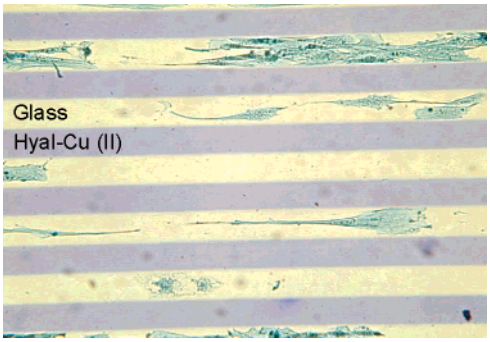

Figure 11. Light micrograph of LEC adhered and aligned on the substrate after 7 days of culture on Hyal−Cu (II) 100 μm microstripes on aminosilanised glass.

assay (Figure 7) and by the fact that BAEC initially adhering to aminosilanised glass, eventually move to Hyal−Cu (II) microstripes (Figure 8). The two different methods employed to realize Hyal−Cu (II) microstructures gave similar results.

The other endothelial cells tested, LEC, did not move from aminosilanised glass to Hyal−Cu (II) microstripes (Figure 11). So, the ability of Cu (II) to induce cell migration and proliferation appears to be limited to blood vascular endothelial cells. It is known that the metal-ion complex has no effect on cells other than endothelial like human fibroblasts or smooth muscle cells.[22] Whether this is due to a specific receptor for Cu (II) on the surface of blood vascular endothelial cells or to a specific intracellular target for Cu (II) which is only present in blood vascular endothelial cells is still unclear.[23] The specific activity of cupric ions on blood vascular endothelial cells may be related to a physiologic mechanism in which these cells are the first to respond to angiogenic stimuli, whereas smooth muscle cells and fibroblasts are activated only after endothelial tubuli are formed.[24]

Why LEC behave differently from BAEC on Hyal−Cu (II) micropatterned surfaces is still to be determined. It must be considered that the two cell types differ in gene expression. Lymphatic commitment of vascular precursors during development depends on the homeobox transcription factor Prox-1.[25] Targeted deletion of the Prox-1 gene specifically inhibits lymphatic vessel formation without affecting blood vasculature. When overexpressed in vitro, Prox-1 is able to re-program blood into lymphatic endothelial cells.[26]

In the field of angiogenesis, different vascular endothelial growth factors (VEGF) act on blood and lymphatic endothelial cells. The best known of these factors, VEGF-A, mainly stimulates blood endothelial cells. Two more recently discovered members of the family, VEGF-C[27,28] and VEGF-D,[29] are instead specific for lymphatic endothelium. It has been demonstrated that copper induces vascular endothelial growth factor expression.[30] To the best of our knowledge, no information is yet available on the effect of copper on VEGF-C and VEGF-D expression. Copper shares some of the pathways utilised by hypoxia to induce VEGF expression.[30]

Taken together with these literature data, our present contribution on the influence of Hyal−Cu (II) on endothelial cells, highlights the existence of profound differences between blood and lymphatic endothelial cells and prompts comparative evaluation of the two cell types to better understand the complex response that an angiogenic stimulus may elicit in vivo.

Conclusions

The AFM, SEM, and ToF-SIMS results presented in this work showed that reproducible Hyal−Cu (II) microstructures with both chemical and topographical heterogeneities can be successfully obtained by photoimmobilization following both preparation methods, i.e., photoimmobilization of the $HyalN_3$−Cu (II) complex (method I) and fabrication of Hyal microstripes followed by soaking them in a $CuSO_4$ solution (method II).

The biological data indicate that Hyal−Cu(II) microstructures show a chemotactic effect, since they are able to direct BAEC growth, favoring their adhesion and migration, independently from the preparation method. The ability of Hyal−Cu (II) to induce cell migration and proliferation appears to be limited to blood vascular endothelial cells; LEC, in fact, did not move from the substrate to Hyal−Cu (II) microstripes, even after 7 days of culture.

Acknowledgment. The financial support from MIUR and University of Siena, through FIRB Project RBNE014585, PRIN 2003 Project 2003037472, and University Research Plan Project (PAR 2003), and from Fondazione Monte dei Paschi de Siena is gratefully acknowledged. The authors would like to thank S. Tanevini for preparing the microstructures and S. Mazzuoli for carrying out the atomic absorption analysis

References and Notes

(1) Barbucci, R.; Magnani, A.; Lamponi, S.; Mitola, S.; Ziche, M.; Morbidelli, L.; Bussolino, F. *J. Inorg. Biochem.* **2000**, *81*, 229−237.
(2) Ziche, M.; Jones, J.; Gullino, P. M. *J. Natl. Cancer Inst.* **1982**, *69*, 475−482.
(3) Alessandri, G.; Raju, K. S.; Gullino, P. M. *Cancer Res.* **1983**, *43*, 1790−1797.
(4) Raju, K. S.; Alessandri, G.; Ziche, M.; Gullino, P. M. *J. Natl. Cancer Res. Inst.* **1982**, *69*, 1183−1188.
(5) Guo-fu, H. *J. Cell. Biochem.* **1998**, *69*, 326−335.
(6) Gullino, P. M.; Ziche, M.; Alessandri, G. *Cancer Metastasis Rev.* **1990**, *9*, 239−251.
(7) Barbucci, R.; Lamponi, S.; Magnani, A.; Peluso G.; Petillo, O. *Polym. Adv. Technol.* **2001**, *12*, 271−278.
(8) Badet, J.; Soncin, F.; N'Guyen, T.; Barritault D. *Blood Coagul. Fibrinolysis* **1990**, *1*, 721−724.
(9) Wiedlocha, A. *Arch. Immunol. Ther. Exp.* **1999**, *47*, 299−305.
(10) Barbucci, R.; Leone, G.; Magnani, A.; Montanaro, L.; Arciola, C. R.; Peluso, G.; Petillo O. *J. Mater. Chem.* **2002**, *12*, 3084−3092.
(11) Barbucci, R.; Magnani A. *Macromol. Symp.* **2000**, *156*, 239−251.
(12) Yoshihiro, I. *Biomaterials* **1999**, *20*, 2333−2342.
(13) Barbucci, R.; Magnani, A.; Lamponi, S.; Pasqui, D.; Bryan S. *Biomaterials* **2003**, *24*, 915−926.
(14) Barbucci, R.; Lamponi, S.; Magnani, A.; Pasqui D. *Biomol. Eng.* **2002**, *19*, 161−170.
(15) Matsuda, T.; Sugawara T. *J. Biomed. Mater. Res.* **1996**, *32*, 165−173.
(16) Flemming, R. G.; Murphy, C. J.; Abrams, G. A.; Goodman, S. L.; Nealey P. F. *Biomaterials* **1999**, *20*, 165.
(17) Magnani, A.; Priamo, A.; Pasqui, D.; Barbucci R. *Mater. Sci. Eng.* **2003**, *C 23*, 315−328.
(18) Beaty, R. D.; Kerber, J. D. *Concepts, Instrumentation and Techniques in Atomic Absorption Spectrophotometry*; The Perkin-Elmer Corporation: Norwalk, CT, 1993.
(19) Weber, E.; Lorenzoni, P.; Lozzi, G.; Sacchi G. *In vitro Cell. Dev. Biol.* **1994**, *30A*, 287−288.
(20) Greco, R. M.; Iocono, J. A. *J. Cell. Physiol.* **1998**, *177*, 465−473.
(21) Magnani, A.; Silvestri, V.; Barbucci R. *Macromol. Chem. Phys.* **1999**, *200*, 2003−2014.

(22) McAuslan, B. R.; Gole, G. A. *Tran. Ophthalmol. Soc. U.K.* **1980**, *100*, 354−358.
(23) Gullino, P. M. In *Angiogenesis: Key Principles, Science, Technology, Medicine*; Steiner, R., Weisz, PB., Lager, R. Eds.; Birkhäuser Verlag: Basel, **1992**; p 125.
(24) Vikkula, M.; Boon, L. M.; Carraway, K. L., III; Kalvert, J. T.; Diamonti, A. J.; Gumnerv, B.; Pasyk, K. A.; Marchuk, D. A.; Warman, M. L.; Cantley, M. C.; Mulliken, J. B.; Olsen, R. B. *Cell* **1996**, *87*, 1181−1190.
(25) Wigle, J. T.; Harvey, N.; Detmar, M.; Lagutina, I.; Grosveld, G.; Gunn, M. D.; Jackson, D. G.; Oliver, G. *EMBO J.* **2002**, *21*, 1505.
(26) Petrova, T. V.; Makinen, T.; Makela, T. P.; Saarela, J.; Virtanen, I.; Ferrell, R. E.; Finegold, D. N.; Kerjaschky, D.; Yla-Herttuala, S.; Alitalo, K. *EMBO J.* **2002**, *21*, 4593.
(27) Joukov, V.; Pajusola, K.; Kaipanen, A.; Chilov D.; Lahtinen I.; Kukk E.; Saksela O.; Kalkkinen N.; Alitalo K. *EMBO J.* **1996**, *15*, 1751.
(28) Jeltsch, M.; Kaipainen, A.; Joukov, V.; Meng X.; Lakso M.; Rauvala H.; Swartz M.; Fukumura D.; Jain R. K.; Alitalo K. *Science* **1997**, *276*, 1423−1425.
(29) Orlandini, M.; Marroncini, L.; Ferruzzi, R.; Oliviero, S. *Proc. Natl. Acad. Sci. U.S.A.* **1996**, *93*, 11675−11680.
(30) Sen, C. K.; Khanna, S.; Venojarvi, M.; Trikha, P.; Ellison, E. C.; Hunt, T. K.; Roy, S. *Am. J. Physiol. Heart Circ. Physiol.* **2002**, *282*, H1821−H1827.

BM049568G